IEEE Access
Multidisciplinary | Rapid Review | Open Access Journal

Received August 13, 2017, accepted September 6, 2017, date of publication September 15, 2017,
date of current version October 12, 2017.

Digital Object Identifier 10.1109/ACCESS.2017.2752903

Novel Wideband Absorptive Bandstop Filters With Good Selectivity

SHIH-HUAN CHIEN[1] AND YO-SHEN LIN[2], (Senior Member, IEEE)
[1]Microelectronics Technology Inc., Hsinchu 300, Taiwan
[2]Department of Electrical Engineering, National Central University, Taoyuan 320, Taiwan

Corresponding author: Yo-Shen Lin (yslin@ee.ncu.edu.tw)

This work was supported in part by the Ministry of Science and Technology, Taiwan, under Grant 105-2221-E-008-021-MY3 and in part by the National Center for High-Performance Computing, Taiwan.

ABSTRACT This paper presents a new type of wideband absorptive bandstop filter (ABSF) design that is capable of absorbing the input power within the stopband at its Port 1. It is achieved by introducing one additional resistor to a conventional wideband stub bandstop filter. Suitable design procedures are established to facilitate the synthesis of the proposed wideband ABSFs with different filter orders and stopband bandwidths. To validate the proposed design method, microstrip ABSF design examples with a stopband center frequency f_0 of 2 GHz and 30-dB stopband bandwidths ranging from 12% to 42% are demonstrated. The measured stopband rejection at f_0 is larger than 60 dB for all design examples. In addition, good input return losses both in the passband and stopband are achieved, and the measured input return loss is better than 10 dB from dc to $2.5f_0$. Larger than 90% of the input power within the stopband can thus be dissipated by the proposed ABSF. To the best of our knowledge, these are the ABSFs with the widest stopband bandwidth ever reported.

INDEX TERMS Bandstop filter, filter synthesis, absorptive stopband.

I. INTRODUCTION

Bandstop filters (BSF) are commonly used for rejecting unwanted blocking and interference signals in RF/microwave systems. Most of the conventional BSF designs are reflective ones, so the unwanted signals are reflected by the BSF. However, the large reflected power is sometimes undesirable for it may lead to performance degradations of adjacent circuit components. A reflectionless BSF or absorptive BSF (ABSF) that can absorb unwanted signals in the stopband thus becomes a favorable choice. Several ABSF designs have been proposed in recent years. In [1] and [2], the lumped-element bridged-T notch filter technique [3], [4] is extended to form first-order absorptive microwave notch filters, in which the signal cancellation between multiple signal paths is utilized to achieve BSF with an absorptive stopband as well as an infinite attenuation. Built upon the perfect notch concept in [1], lossy all-pass networks are used to implement perfectly-matched BSFs in [5]. In [6], a new class of reflectionless filter is proposed, and lumped-element filter prototypes with theoretically perfect input and output matchings at all frequencies are demonstrated. They are then converted to transmission line-based ones in [7] so as to be better suited for high-frequency designs. On the other hand, a lumped-element realization of the ABSF design concept in [2] is presented in [8] to achieve a more compact circuit size. In [9], a multi-harmonic absorption filter is realized by the combination of a multi-band rejection filter and a terminated broadband bandpass filter, and it is targeted for the harmonic absorption of a power amplifier such that the instability issue generated by the reflected harmonics can be avoided. In [10] and [11], narrowband ABSFs based on introducing one lossy resonator to the conventional coupled-line BSF is proposed. They are targeted for absorbing the LO-to-RF leakage of mixer in a heterodyne receiver so as to prevent the degradation of mixer's conversion gain. Recently in [12], a quasi-lumped bridged-T ABSF, similar to Bode's original design in [3] and [4], is proposed to achieve large attenuation while maintaining a small circuit size. In order to protect sensitive receivers of reconfigurable RF front-ends, ABSFs with a tunable stopband have also been demonstrated in [2], [13]–[17].

Most of the previous works on ABSF designs utilize the signal cancellation between multiple signal paths to achieve high rejection. Therefore, they exhibit first-order bandstop responses with relatively narrow stopband bandwidths up to only a few percent. As an example, the analysis in [16]

shows that the stopband attenuation bandwidth increases with the decreasing Q-factor of the resonator, and the maximal achievable 30-dB rejection bandwidth is less than 7% even for $Q = 1$. On the other hand, acoustic wave resonators have also been introduced to achieve ABSF designs with an ultra-narrow stopband bandwidth [18], [19]. For applications such as the harmonic suppression of nonlinear active circuits or the LO leakage suppression of wideband mixers, a wider absorptive stopband is desired. The cascade of multiple first-order ABSFs has been suggested to achieve a wider stopband bandwidth in [20]–[22]. However, the resulted stopband bandwidth is still narrow and the stopband rejection within the stopband is not all large due to the equal-ripple stopband response. In addition, since the perfect impedance match condition of the ideal ABSF is not achievable in practice due to the presence of parasitic effects, the implemented cascaded ABSF design does not achieve good return loss responses both in the passband and the stopband. In [23], a bandwidth-enhanced ABSF based on the lumped-element realization of the 2nd-order lossy filter topology [21] is proposed, and it achieves a 20-dB rejection bandwidth of 12% and a 40-dB rejection bandwidth of 1.6%. Its bandwidth and frequency selectivity are both better than conventional first-order designs, e.g., [8], but the achieved stopband bandwidth is still not wide.

In this work, a simple and effective way is proposed to achieve wideband ABSFs with a 40-dB stopband bandwidth up to 31.8%. It is based introducing one resistor to the conventional wideband optimal microwave BSF [24]–[27] so as to absorb the input power at its Port 1 within the stopband. The synthesis method and design equations of proposed wideband ABSF are given in Section II. The realizable bandwidth and filter order are also investigated along with proper design modifications under practical design considerations. Microstrip ABSF design examples are demonstrated in Section III to validate the proposed design theory, and good measured performances are achieved.

II. FILTER DESIGN

A. BASIC CIRCUIT MODEL AND DESIGN PROCEDURE

Shown in Fig. 1(a) is the basic circuit model of proposed wideband ABSF. It is based on introducing one lossy resonator to a conventional wideband stub BSF consisting of quarter-wavelength ($\lambda/4$) open stubs and $\lambda/4$ connecting lines. To achieve a more compact circuit size and more uniform stub impedances, the optimal microwave BSF [24]–[26] is the preferred choice for implementing the wideband stub BSF. It is optimal because the $\lambda/4$ connecting lines, i.e., the unit elements between stubs in Fig. 1(a) are incorporated in the design such that significantly steeper attenuation characteristics can be obtained for the same number of stubs than is possible for stub BSFs designed with redundant unit elements [26], [27]. Specifically, an optimal microwave BSF with n stubs features a $(2n-1)$th order bandstop response.

The operation principle of proposed wideband ABSF is explained as follows. Since all transmission line sections

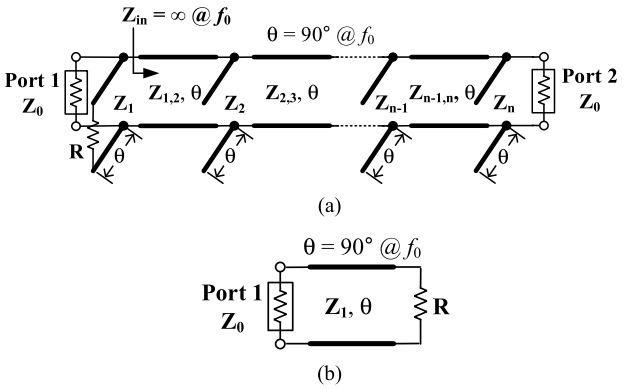

FIGURE 1. (a) Basic circuit model of the proposed wideband absorptive bandstop filter (ABSF), which is achieved by introducing one lossy resonator to a conventional stub bandstop filter (BSF). (b) Its equivalent-circuit model at the stopband center frequency f_0.

in Fig. 1(a) are $\lambda/4$ long, the input impedance Z_{in} looking into the right-hand side of the first shunt open stub is infinite at the stopband center frequency f_0. Therefore, the filter circuit model at f_0 can be further simplified as Fig. 1(b). To have the resistor R absorb all the input power at Port 1, its value is set according to

$$R = Z_1^2/Z_0 \tag{1}$$

by using the well-known $\lambda/4$ transformer design formula. In this way, a bandpass response centered at f_0 can be obtained for the circuit model in Fig. 1(b) when the resistor R is considered as the output termination, which is similar to the design concept of [11]. As a result, the input power at f_0 will not propagate to Port 2 of the wideband ABSF in Fig. 1(a) due to the infinite Z_{in}, but it will be totally consumed by the resistor R instead.

The design procedure of proposed wideband ABSF can be summarized as follows. First, the resistor is neglected (i.e., $R = \infty$) and the stub BSF is designed as a reflective one using the design tables available in [27]. Specifically, the line impedances are determined by

$$\begin{aligned} Z_i &= Z_0/g_i \\ Z_{i,i+1} &= Z_0/J_{i,i+1} \end{aligned} \tag{2}$$

where Z_0 is the port reference impedance while g_i and $J_{i,i+1}$ are the element values of optimal microwave BSF. Next, the resistor R is introduced and its initial value is given by (1). To illustrate the achievable performance, a proposed wideband ABSF with four stubs (i.e., $n = 4$) is designed with a stopband center frequency $f_0 = 2$ GHz, a fractional bandwidth (FBW) $= 0.5$, and a Chebyshev response with a ripple constant $\varepsilon = 0.1005$. The reference impedances of Port 1 and 2 are both set as $Z_0 = 50\ \Omega$. By referring to the element value table in [27], the line impedances can be determined by (2) as $Z_1 = Z_4 = 123.86\ \Omega$, $Z_2 = Z_3 = 69.33\ \Omega$, $Z_{12} = Z_{34} = 60.84\ \Omega$, and $Z_{23} = 63.21\ \Omega$. The initial value of R can then be calculated using (1) to give $R = 306.85\ \Omega$.

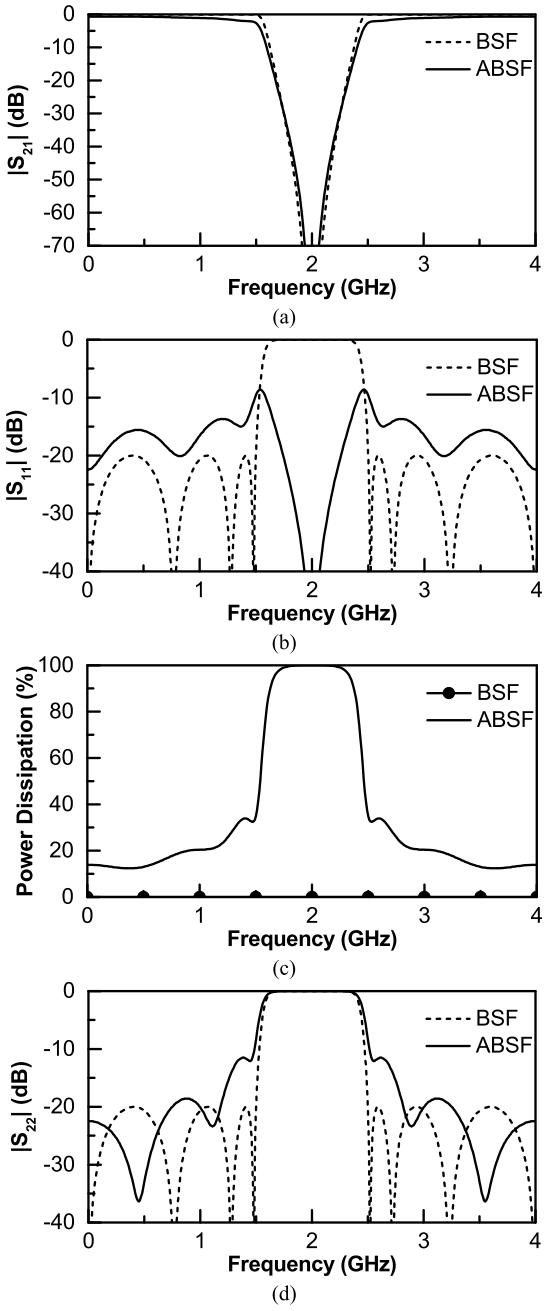

FIGURE 2. Circuit simulated (a) $|S_{21}|$ and (b) $|S_{11}|$ frequency responses of a proposed wideband ABSF design example ($f_0 = 2$ GHz, FBW = 0.5 and $n = 4$) and its reflective BSF counterpart. (c) Power dissipated in the ABSF with the input at Port 1, which is calculated by $1 - |S_{11}|^2 - |S_{21}|^2$. (d) Output reflection coefficient $|S_{22}|$ at Port 2.

Shown in Fig. 2 are the circuit simulated S-parameters of this wideband ABSF, and those for its reflective BSF counterpart (i.e., $R = \infty$) is also included for comparison. As observed in Fig. 2(a), the proposed wideband ABSF exhibits a bandstop response centered at $f_0 = 2$ GHz. The insertion loss response is very similar to that of the reflective BSF except for some degradation at the two stopband edges. Still, good selectivity is achieved for the proposed wideband ABSF since the reflective BSF with four stubs features a 7th-order Chebyshev response. The 30-dB rejection bandwidth of the wideband ABSF is from 1.75 to 2.25 GHz or 25%, and it is almost identical to that of the reflective BSF. On the other hand, the ABSF's input reflection coefficient $|S_{11}|$ in Fig. 2(b) is equal to zero or $-\infty$ dB at f_0 while that of the reflective BSF is equal to one or 0 dB. As a result, in Fig. 2(c) the power dissipated by the wideband ABSF is 100% at f_0, while it is zero at all frequencies for the conventional reflective BSF. This verifies that the proposed wideband ABSF can successfully absorb the input power at f_0 by introducing the additional resistor R. As the frequency moves away from f_0, the $|S_{11}|$ of the proposed wideband ABSF increases until a maximal value is reached. This is because Z_{in} in Fig. 1(a) is infinite only at f_0 and $R = Z_1^2/Z_0$ can only achieve perfect impedance matching at f_0 in Fig. 1(b). As a result, the power dissipation also reduces as the frequency moves away from f_0. As for the output reflection coefficient $|S_{22}|$ shown in Fig. 2(d), the proposed wideband ABSF exhibits a similar response to that of the conventional reflective BSF because no lossy resonator is used at the output port.

According to Fig. 2(b), the $|S_{11}|$ of this proposed wideband ABSF exceeds -10 dB at the two stopband edges, which may not be acceptable for some applications. This can be improved by modifying the resistance of R. Shown in Fig. 3 is the input impedance Z_{inR} looking into the open end of the first open stub where R is connected to. It can be observed that Z_{inR} is purely resistive at $f_0 = 2$ GHz with a value of 306.85 Ω. As the frequency moves away from f_0, Z_{inR} becomes a complex value and $|Z_{inR}|$ becomes higher than its value at f_0. This is the cause of the larger $|S_{11}|$ at the two stopband edges where $|Z_{inR}|$ becomes higher than 306.85 Ω, since the resistor $R = Z_1^2/Z_0$ no longer matched to Z_{inR} there. It also implies that the $|S_{11}|$ at the stopband edges can be simply improved by increasing the value of R at the expense of some increase in $|S_{11}|$ at f_0.

Shown in Fig. 4 are the circuit simulated input reflection coefficients of this wideband ABSF design under different values of R. As R increases from the initial value of 306.85 Ω, it can be found that the input reflection coefficient $|S_{11}|$ at f_0 increases due to impedance mismatch. However, the maximal input reflection coefficients at the two stopband edges decrease as R increases. Especially, when R increases to 516.85 Ω, the maximal $|S_{11}|$ reduces to a level that is about equal to the reflection coefficient at f_0, and a nearly equal-ripple $|S_{11}|$ response within the stopband is obtained. In addition, the $|S_{11}|$ at all frequencies are now below -11.87 dB. On the other hand, the $|S_{21}|$ response does not change much with the varying resistance. This can be examined in detail by referring to the comparison between the two extreme cases with $R = 306.85$ and 516.85 Ω in Fig. 5. By increasing R from 306.85 to 516.85 Ω, the maximal $|S_{11}|$ is reduced from -8.62 to -11.87 dB as expected, while the difference in $|S_{21}|$ between the two cases is negligible as shown in Fig. 5(a). According to Fig. 5(c), the power dissipation at f_0 reduced from 100% to 93.5% after R increases to 516.85 Ω. Anyway,

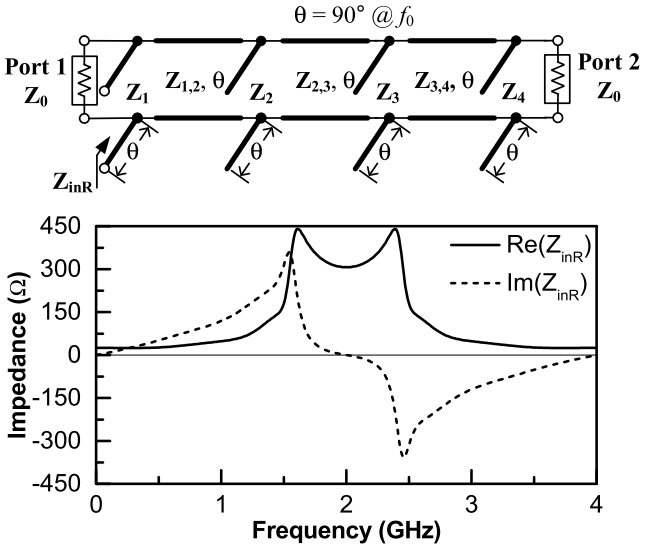

FIGURE 3. Circuit simulated input impedance Z_{inR} looking into the open end of the first open stub of the wideband ABSF with $f_0 = 2$ GHz, FBW = 0.5 and $n = 4$.

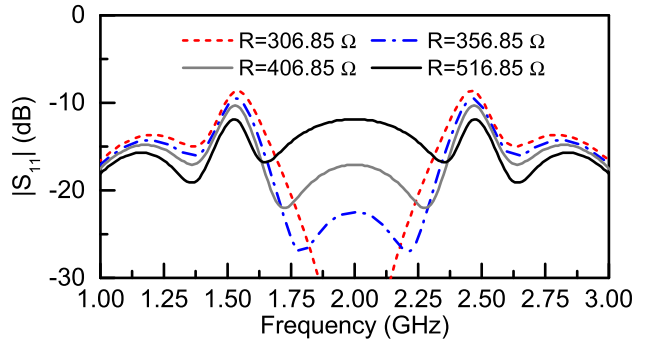

FIGURE 4. Effect of R on the circuit simulated $|S_{11}|$ frequency response of the proposed wideband ABSF with $f_0 = 2$ GHz, FBW = 0.5 and $n = 4$.

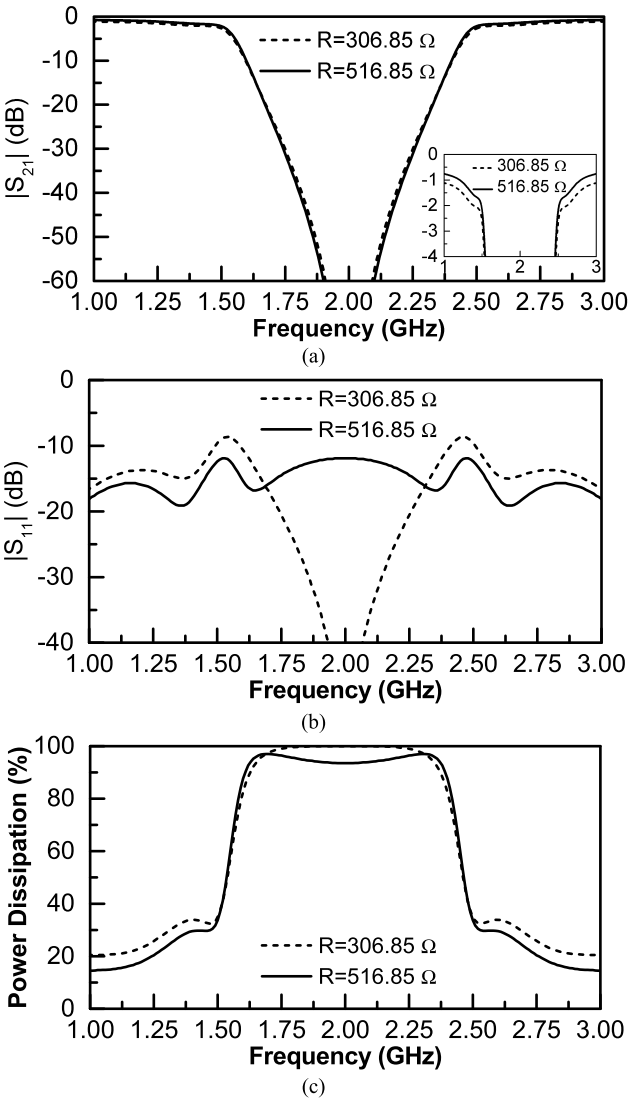

FIGURE 5. Effect of R on the bandstop performance of the wideband ABSF design example ($f_0 = 2$ GHz, FBW = 0.5 and $n = 4$) for R = 306.85 and 516.85 Ω. Circuit simulated (a) $|S_{21}|$ and (b) $|S_{11}|$ frequency responses. (c) Power dissipated in the ABSF with the input at Port 1.

the bandwidth for larger than 93.5% power dissipation is from 1.626 to 2.374 GHz (or 37.4%) while the reflected power is less than 6.5% in the same frequency range, which is considered as acceptable for most applications.

In addition to an absorptive stopband, a good passband performance is also obtained for this proposed wideband ABSF after R increases to 516.85 Ω. This is because the value of resistive loading R is now closer to that of the original reflective BSF, i.e., R $= \infty$. According to the wideband frequency response in Fig. 6, it exhibits a passband with better than 1 dB insertion loss from dc to 1.2 GHz and from 2.8 to 5.2 GHz. The corresponding passband input/output return losses are all better than 15.87 dB, while the input return loss at Port 1 is better than 11.87 dB at all frequencies. Repeated absorptive stopbands at odd multiples of f_0 are observed due to the periodic property of the original optimal microwave BSF. Therefore, increasing the resistance of R until an equal-ripple $|S_{11}|$ around f_0 is reached is considered as the final step of the design procedure of the proposed wideband ABSF. Still, R is a free variable the designer can use to trade off between the return loss at f_0 and the minimum in-band return loss depending on the application requirement.

The proposed wideband ABSF is targeted for the harmonic absorption of nonlinear devices, e.g., a power amplifier. Therefore, only one lossy resonator is introduced near the input port, i.e. Port 1, which will be connected to the output port of a power amplifier. Although multiple lossy resonators can also be used, a single lossy resonator at Port 1 is sufficient to achieve the required harmonic absorption while maintaining minimum degradation on the passband insertion loss and stopband selectivity as demonstrated in this design example.

B. PARAMETRIC ANALYSIS

Although the proposed design method starts from the condition of Z_{in} in Fig. 1(a) equals infinity at the stopband center frequency only, the resulted ABSF can handle

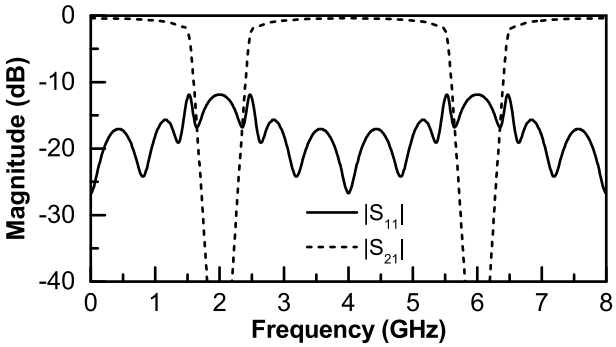

FIGURE 6. Wideband circuit simulated frequency response of the proposed ABSF design example ($f_0 = 2$ GHz, FBW = 0.5 and $n = 4$) with R = 516.85 Ω.

TABLE 1. Circuit parameters of The four ABSFs with four stubs in Fig. 7.

FBW	R (Ω)	Z_1=Z_4 (Ω)	Z_2=Z_3 (Ω)	Z_{12}=Z_{34} (Ω)	Z_{23} (Ω)
0.3	1499	216.74	123.78	53.54	54.74
0.5	516.85	123.86	69.33	60.84	63.21
0.7	246.22	82.83	45.54	70.32	74.28
0.9	151.13	62.94	34.09	80.61	86.28

TABLE 2. Performances of the four ABSFs with four stubs in Fig. 7.

FBW	30-dB Stopband Bandwidth	Bandwidth for >90% Power Dissipation	Max. Input Reflection Coeff.	Min. Passband Insertion Loss
0.3	13.6%	22.1%	-12.78 dB	0.14 dB
0.5	25.8%	39.8%	-11.87 dB	0.41 dB
0.7	41.2%	60.8%	-10.92 dB	0.84 dB
0.9	56.2%	80.6%	-10.1 dB	1.33 dB

a 30-dB stopband bandwidth from about 12% to 42% according to the following analysis. Fig. 7 compares the circuit simulated frequency responses of several proposed wideband ABSF designs with four stubs (i.e., $n = 4$) and different FBWs ranging from 0.3 to 0.9. Here, FBW refers to the ripple bandwidth of the optimal microwave BSF designed with a Chebyshev response and a ripple constant $\varepsilon = 0.1005$. The circuit parameters are obtained using (2) and the design tables in [27], and the results are listed in Table 1. Notably, the resistance of R for all cases have been increased from the initial value given by (1) to the value in Table 1 so as to achieve an equal-ripple $|S_{11}|$ response around f_0 as described in the previous subsection.

All four designs in Fig. 7 demonstrate a bandstop response with an absorptive stopband, and their performances are summarized in Table 2. According to Fig. 7(a) and 7(c), the bandwidths of 30-dB stopband rejection for the four designs with FBW = 0.3, 0.5, 0.7 and 0.9 are equal to 13.6, 25.8, 41.2, and 56.2% respectively, while the bandwidths for larger than 90% power dissipation are equal to 22.1, 39.8, 60.8, and 80.6%, respectively. However, it can be observed from Fig. 7(b) that the maximal input reflection coefficient gradually increases as FBW increases. Specifically, the design with FBW = 0.9

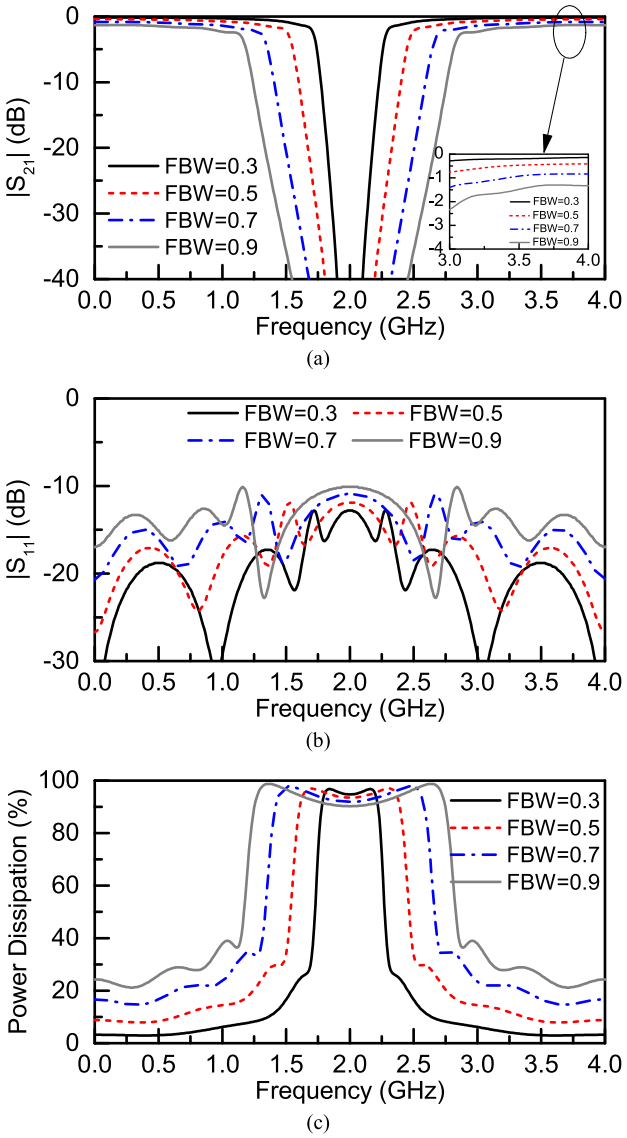

FIGURE 7. Circuit simulated (a) $|S_{21}|$ and (b) $|S_{11}|$ frequency responses of proposed wideband ABSF with $n = 4$ and $f_0 = 2$ GHz but different FBWs. (c) Power dissipated in the ABSF with the input at Port 1.

may be considered as the upper limit of realizable FBW because its maximal $|S_{11}|$ already reaches −10.1 dB. In addition, the minimum passband insertion loss at dc and $2f_0$ also increases with FBW according to Table 2. This also limits the maximal realizable FBW of proposed wideband ABSF.

On the other hand, the problem with smaller FBWs is that the required line impedance becomes abnormally high such that it may not be realizable in practice, which is a common issue for stub BSF structures. For the case with FBW = 0.3 in Table 1, the maximal line impedance is equal to 216.74 Ω and it is not realizable using planar transmission line structures. Therefore, a modified design approach will be proposed to deal with this issue in the next subsection, i.e. Section II.C so as to extend the lower bound of realizable FBW for the proposed wideband ABSF.

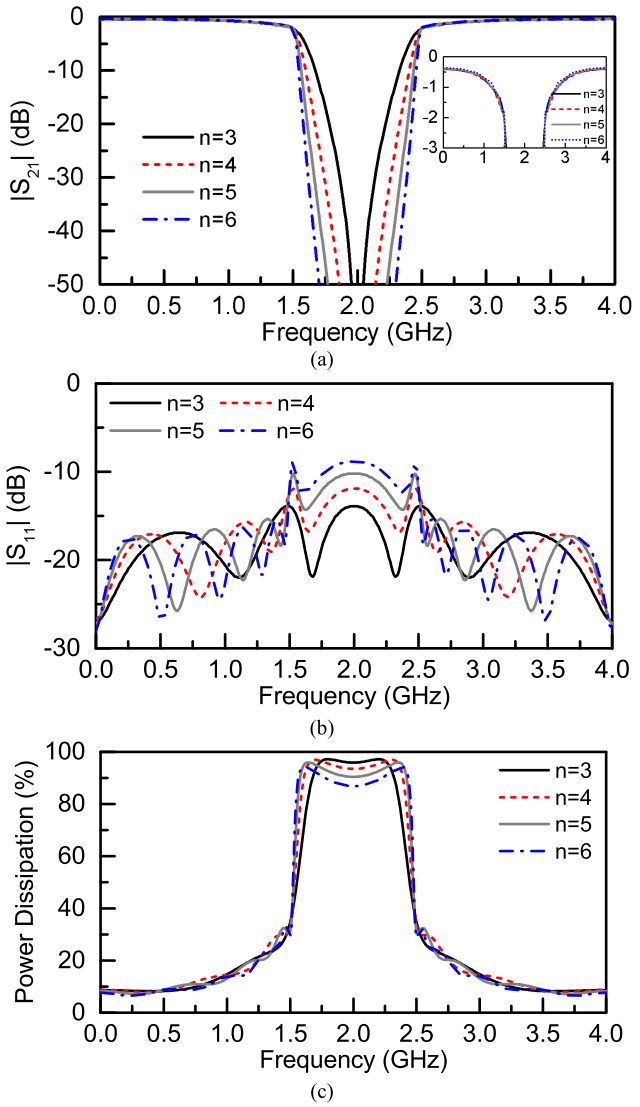

FIGURE 8. Circuit simulated (a) $|S_{21}|$ and (b) $|S_{11}|$ frequency responses of proposed wideband ABSF with $f_0 = 2$ GHz, FBW = 0.5 but different number of stubs. (c) Power dissipated in the ABSF with the input at Port 1.

Fig. 8 compares the circuit simulated results of proposed wideband ABSFs with the same FBW of 0.5 but different numbers of shunt stubs (i.e., n), which means different filter order. The circuit parameters are listed in Table 3, and the resistance R for each case has been increased again to achieve an equal-ripple input reflection coefficient around f_0. According to Fig. 8, the frequency selectivity increases with the number of stubs n as expected. The shape factor (i.e., 3-dB rejection bandwidth/30-dB rejection bandwidth or RBW_{3-dB}/RBW_{30-dB}) for the four cases with $n = 3$, 4, 5, and 6 are equal to 3.30, 1.85, 1.44, and 1.27 respectively. However, it is found that the maximal $|S_{11}|$ also increases with n. For $n = 6$, the maximal $|S_{11}|$ already exceeds -10 dB, which may not be considered as usable in practice. For $n = 5$, it is equal to -10.2 dB and this barely passes the common requirement on input return loss. Although it seems that the frequency selectivity of proposed wideband ABSF is therefore limited due to the increase of maximal $|S_{11}|$ with n, a modified design will be proposed in Section II.D to improve the input reflection coefficient for larger n such that a highly selective wideband ABSF with proper input impedance matching can still be achieved.

TABLE 3. Circuit parameters of proposed ABSF designs with different number of stubs in Fig. 8.

n	3	4	5	6
R (Ω)	528.78	516.85	549.74	601.40
Z_1 (Ω)	132.43	123.86	120.36	118.61
Z_2 (Ω)	78.99	69.33	66.40	65.12
Z_3 (Ω)	132.43	69.33	62.24	60.13
Z_4 (Ω)	-	123.86	66.40	60.13
Z_5 (Ω)	-	-	120.36	65.12
Z_6 (Ω)	-	-	-	118.61
Z_{12} (Ω)	59.55	60.84	61.41	61.70
Z_{23} (Ω)	59.55	63.21	64.42	64.94
Z_{34} (Ω)	-	60.84	64.42	65.54
Z_{45} (Ω)	-	-	61.41	64.94
Z_{56} (Ω)	-	-	-	61.70

C. DESIGN MODIFICATION FOR ABSF WITH MODERATE BANDWIDTH

The proposed wideband ABSF is based on the conventional optimal microwave BSF that employs the stub BSF structure. Therefore, it is more suitable for wideband designs because the line impedance becomes unreasonably high if the required stopband bandwidth is very narrow, which has been shown in Table 1. On the other hand, due to the lowpass to bandstop transformation used in microwave filter synthesis, the frequency selectivity decreases as the stopband bandwidth increase for the same number of stubs, i.e., the same circuit size. Therefore, in case that the required stopband bandwidth is not large, a moderate bandwidth ABSF is preferred due to the better frequency selectivity. A modified design approach to reduce the required line impedance is developed here so as to ease the realization of proposed ABSF with moderate bandwidth.

Size reduction of transmission line through the use of capacitive or inductive loadings has been widely adopted for the development of compact microwave passive circuits. As pointed out in [28], when a line is inductively loaded, not only the line length but also the characteristic impedance of the line must be decreased in order to maintain the total capacitance and inductance of the original line. This property can be used to solve the issue of high line impedance for the proposed ABSF with moderate bandwidth. Specifically, the stubs in the proposed ABSF with a line impedance Z_i that is too large can be modified to the inductor-loaded ones shown in Fig. 9. The required inductance L, line impedance Z_{iL}, and line length θ_{iL} can be determined according to [28] as:

$$Z_{iL} = Z_i \sin\theta_{iL}$$
$$L = \frac{Z_i}{\omega_0}\cos\theta_{iL} \tag{3}$$

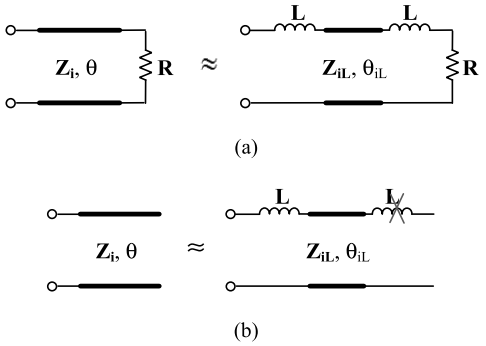

FIGURE 9. Design modifications of the (a) resistor loaded stub and (b) open stub in the proposed wideband ABSF in case that the line impedance Z_i is higher than the maximal realizable impedance.

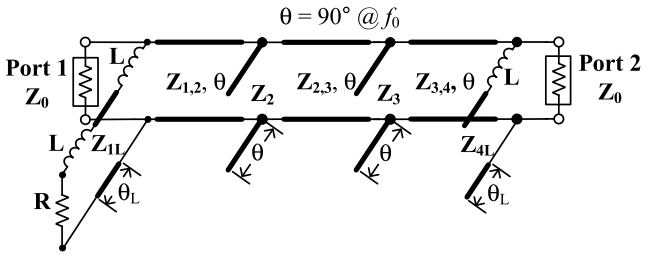

FIGURE 10. Modified design-I of proposed ABSF of moderate bandwidth for $n = 4$.

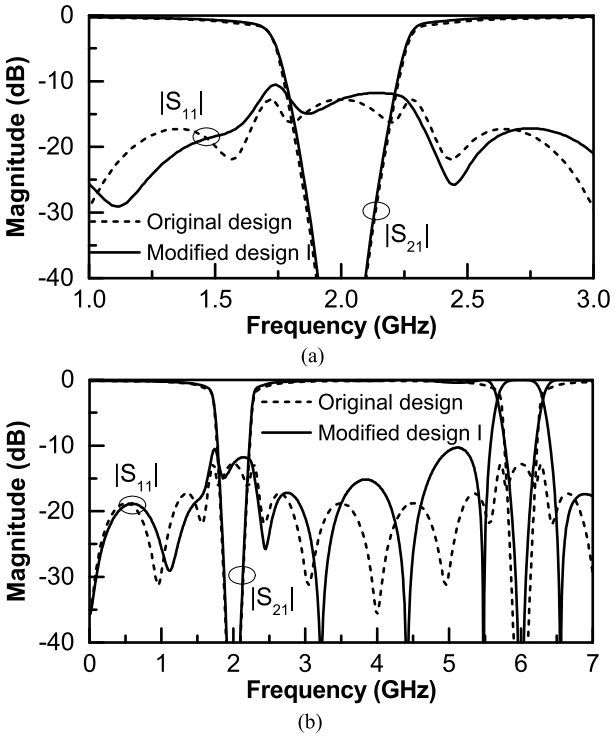

FIGURE 11. Circuit simulated results for the modified design-I of proposed ABSF in Fig. 10 and the original design with $f_0 = 2$ GHz, FBW = 0.3, and $n = 4$. (a) Narrowband and (b) wideband S-parameter frequency responses when the input is at Port 1.

According to (3), the line impedance Z_i can be reduced by a factor of $\sin\theta_{iL}$ with the inductor loadings. However, it should be noted that if θ_{iL} is chosen too small, the bandwidths of the two equivalences in Fig. 9 will also reduce. Therefore, it is suggested to set Z_{iL} close to the maximal realizable line impedance of the given fabrication process, and calculate the resulted θ_{iL} and L accordingly.

As a demonstration, shown in Fig. 10 is the modified design-I of proposed ABSF with four stubs (i.e., $n = 4$) based on the equivalences illustrated in Fig. 9. According to the circuit parameters given in Table 1, when FBW $= 0.3$ the first and last shunt stubs require a high line impedance of 216.74 Ω. Therefore, these two stubs are replaced with the inductively loaded ones in Fig. 9 while all other parts of the filter structure remain unchanged. By setting $Z_{iL} =$ 139.3 Ω (i = 1 or 4), the required L and θ_{iL} can be obtained using (3) as 13.2 nH and 60° at $f_0 = 2$ GHz, respectively. Shown in Fig. 11 are the circuit simulated S-parameters of this modified ABSF design-I, and those of the original ABSF design based on Fig. 1 are also included for comparison. The two simulated $|S_{21}|$ responses are almost identical from dc to 5 GHz or $2.5f_0$, which implies that the bandwidths of the two equivalences in Fig. 9 are sufficient for this proposed ABSF design. Although the simulated $|S_{11}|$ of the modified design-I deviates from that of the original ABSF design for $f \neq f_0$, good input impedance matching is still achieved and the simulated $|S_{11}|$ of the modified design-I is better than −10.5 dB from dc to 5.05 GHz. The problem of high line impedance is thus solved, and this extends the lower limit of realizable bandwidth for the proposed ABSF.

D. DESIGN MODIFICATION FOR HIGHER ORDER ABSF

As pointed out in Section II.B, the maximal input reflection coefficient increases with the FBW as well as the number of stubs n. This can be improved by the modified design-II of proposed wideband ABSF shown in Fig. 12, in which the short end of the resistor R is replaced by a λ/4 open stub. According to Fig. 3, the input impedance Z_{inR} looking into the open end of the first open stub is purely resistive at f_0 only. For frequencies below and above f_0, it becomes complex impedances with inductive and capacitive reactances, respectively. Therefore, a single resistor R in the original design cannot achieve wideband impedance matching. By changing R into the combination of R and a λ/4 open stub as shown in Fig. 12, the bandwidth of impedance matching can be improved because the λ/4 open stub is capacitive for $0 < f < f_0$ and it is inductive for $f_0 < f < 2f_0$, while it is equal to an ideal short at f_0. Therefore, by properly setting the line impedance Z_S of the λ/4 open stub, it is possible to achieve conjugate matching at f_0 as well as two other frequency points below and above f_0. In this way, the maximal input reflection coefficient within the stopband can be reduced.

The performance of the modified design-II in Fig. 12 is examined by a proposed wideband ABSF design example with five stubs (i.e., $n = 5$), and the specifications are $f_0 = 2$ GHz, $Z_0 = 50$ Ω, and FBW $= 0.5$. The circuit parameters are those listed in Table 3 for $n = 5$, except

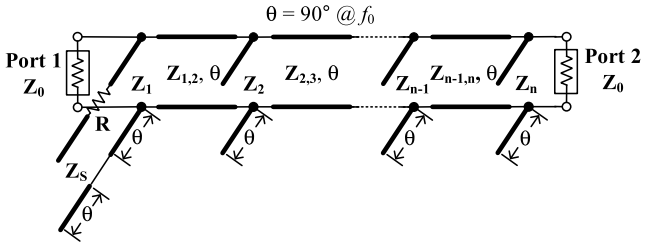

FIGURE 12. Modified design-II of proposed ABSF for improving the input return loss at Port 1 as well as the passband insertion loss.

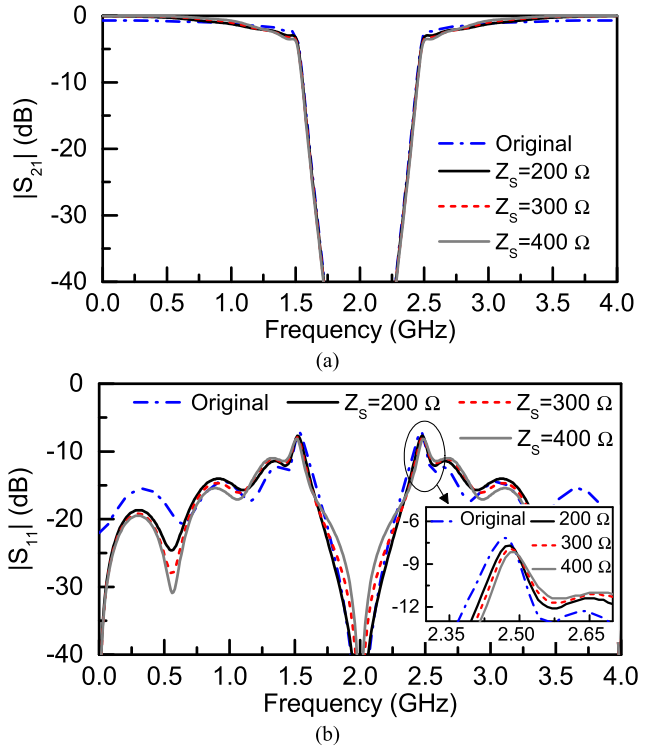

FIGURE 13. Circuit simulated S-parameters of the modified design-II of proposed ABSF in Fig. 12 with $f_0 = 2$ GHz, FBW = 0.5 and $n = 5$ under different line impedance Z_S of the λ/4 open stub. The circuit simulated results of the original ABSF design is also included for comparison. (a) $|S_{21}|$. (b) $|S_{11}|$.

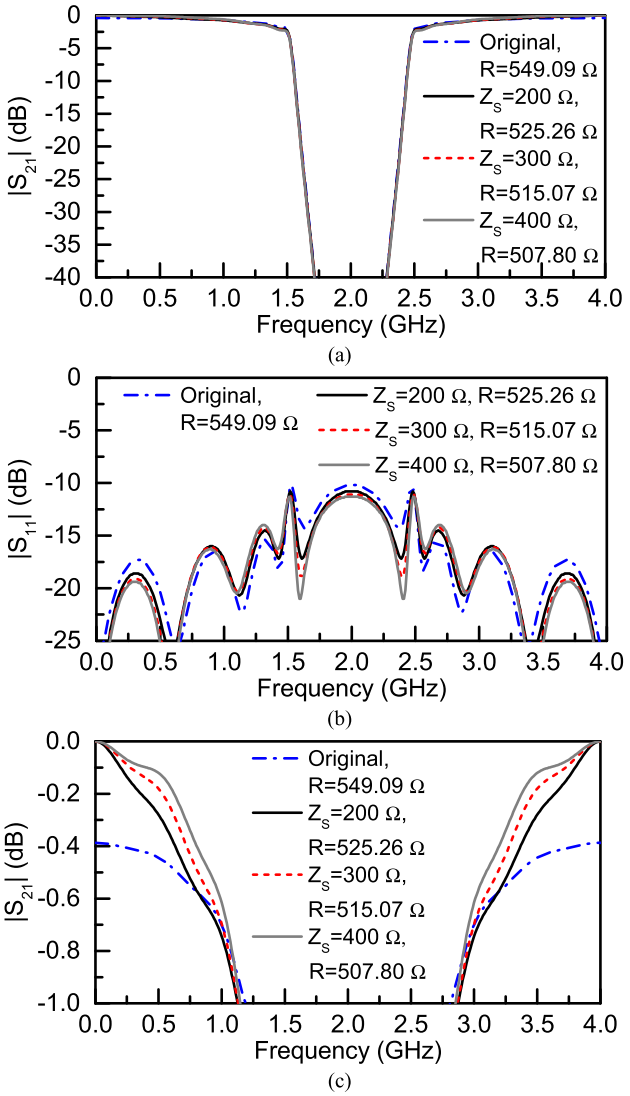

FIGURE 14. Circuit simulated results for the modified design-II of proposed ABSF in Fig. 12 with $f_0 = 2$ GHz, FBW = 0.5, and $n = 5$ under different line impedances Z_S of the λ/4 open stub. The results for the original ABSF design is also included for comparison. The resistance R for each case is increased to the value shown in the figure legend. (a) $|S_{21}|$. (b) $|S_{11}|$. (c) Close-up view of the $|S_{21}|$ responses in the passband.

that the resistance R is calculated using (1) as 289.73 Ω so as to achieve perfect input impedance matching at f_0. Shown in Fig. 13 are the circuit simulated S-parameters of this ABSF under different line impedances Z_S of the λ/4 open stub ranging from 200 to 400 Ω. The results for the original ABSF design, i.e. Fig. 1(a) is also included for comparison, in which the resistor R is terminated to ground instead. It is found that the input reflection coefficient $|S_{11}|$ remains equal to 0 at f_0 for all four cases in Fig. 13 as expected, while the maximal $|S_{11}|$ occurs at the two stopband edges improves slightly for the modified design-II with a λ/4 open stub. In addition, the maximal $|S_{11}|$ reduces as Z_S increases. However, even for the case with $Z_S = 400$ Ω, the maximal $|S_{11}|$ still exceeds −10 dB. Again, to improve the $|S_{11}|$ and achieve a good overall input matching within the stopband, the resistor R can be increased until a nearly equal-ripple $|S_{11}|$ within the stopband is reached. Shown in Fig. 14 are the circuit simulated results of the three modified designs with Z_S equals to 200, 300, and 400 Ω as well as that of the original design, in which the resistances R for them are increased to the value shown in the figure legend. The maximal $|S_{11}|$ of the original ABSF design is now improved to −10.19 dB, while those of the modified designs with a λ/4 open stub are −10.77, −11.05, and −11.26 dB for Z_S equals to 200, 300, and 400 Ω respectively, which are all better than that of the original ABSF design.

Although the improvement in $|S_{11}|$ is not large, there are two additional advantages of the modified design-II with a λ/4 open stub shown in Fig. 12. First, according to Fig. 14(c) the passband insertion loss becomes substantially smaller

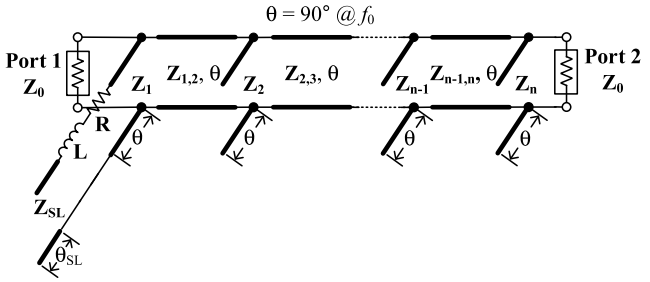

FIGURE 15. Modified design-III of proposed ABSF for improving the input return loss at Port 1 as well as the passband insertion loss.

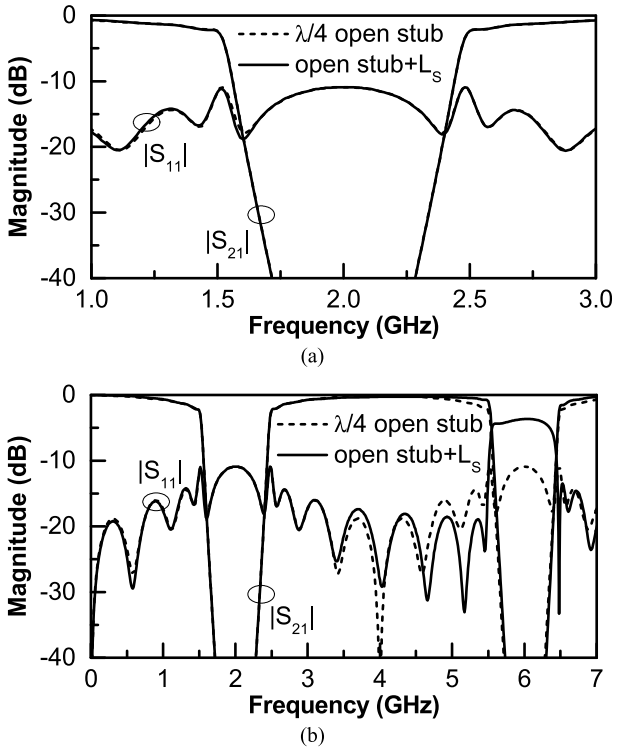

FIGURE 16. Circuit simulated frequency responses of the modified design-II and -III with n = 5, f_0 = 2 GHz, FBW = 0.5, and Z_0 = 50 Ω. (a) Narrowband and (b) wideband $|S_{11}|$ and $|S_{21}|$ frequency responses.

than the original ABSF design. This is because the resistor R becomes floating at dc and $2f_0$ such that the insertion loss becomes zero at these two frequencies. Second, no via is required for the modified design-II with a λ/4 open stub, which greatly simplifies the circuit fabrication process.

Even though the modified design-II with a λ/4 open stub can achieve better insertion loss and return loss, a high Z_S larger than 200 Ω is required for a notable improvement in $|S_{11}|$. Since such a high line impedance may not be achievable in practice, a further modification shown in Fig. 15 is proposed, in which the equivalent circuit in Fig. 9(b) is employed. Specifically, the λ/4 open stub is now replaced by the combination of a series inductor L and an open stub of line impedance Z_{SL} and electrical length θ_{SL} at f_0 ($\theta_{SL} < 90°$). According to the discussions in Section II.C, with the introduction of L, one can achieve a higher equivalent line impedance Z_S using a lower line impedance Z_{SL}. Specifically, L, Z_{SL}, and θ_{SL} are related to the equivalent line impedance Z_S of the λ/4 open stub by (4)

$$\begin{aligned} Z_{SL} &= Z_S \sin\theta_{SL} \\ L &= \frac{Z_S}{\omega_0} \cos\theta_{SL} \end{aligned} \tag{4}$$

In order to achieve the largest possible Z_S, Z_{SL} can be set as the highest realizable line impedance for a given fabrication process, while L is selected as the largest inductor whose self-resonance frequency is higher than the upper limit of the required passband. The corresponding Z_S and θ_{SL} can then be obtained by

$$\begin{aligned} \theta_{SL} &= \tan^{-1}\left(\frac{Z_{SL}}{\omega_0 L}\right) \\ Z_S &= Z_{SL} \csc\theta_{SL} \end{aligned} \tag{5}$$

For the fabrication process used in this work, the maximal realizable line impedance is $Z_{SL} = 147.9$ Ω and the largest chip inductor with a self-resonant frequency higher than 5 GHz (or $2.5f_0$) is $L = 15$ nH. The corresponding θ_{SL} is 38.1° at $f_0 = 2$ GHz and the equivalent Z_S is 239.6 Ω according to (5). Fig. 16 compares the circuit simulated frequency responses of proposed modified design-II and -III with $n = 5$, $f_0 = 2$ GHz, FBW = 0.5, and $Z_0 = 50$ Ω. The modified design-II uses a λ/4 open stub of line impedance $Z_S = 239.6$ Ω while the modified design-III employs a 15-nH ideal inductor in series with an open stub with $Z_{SL} = 147.9$ Ω and $\theta_{SL} = 38.1°$ at f_0. The resistor R for both designs are 520.89 Ω so as to achieve a nearly equal-ripple in-band $|S_{11}|$ response as shown in Fig. 16(a), and the maximal $|S_{11}|$ is −10.9 dB. The frequency responses of these two modified designs are almost identical up to 5 GHz, and this validates the effectiveness of the modified design-III in Fig. 15. The modified design-III can thus be used to improve the $|S_{11}|$ and $|S_{21}|$ response of proposed wideband ABSF such that the upper limit of realizable FBW and filter order can be further extended.

III. MICROSTRIP FILTER IMPLEMENTATION

According to the proposed design method in Section II, wideband BSF with an absorptive stopband can be easily designed for a given specification. Four design examples in Section II will be implemented in microstrip form and the performance will be presented in this section.

A. CASE 1: FBW = 0.5 and n = 4

First, the proposed wideband ABSF with $f_0 = 2$ GHz, FBW = 0.5, $n = 4$, and $Z_0 = 50$ Ω in Fig. 5 of Section II.A is implemented in microstrip using a RO4350B substrate ($\varepsilon_r = 3.48$, $\tan\delta = 0.004$, and thickness h = 1.524 mm). The ABSF is designed based on an optimal microwave BSF with a Chebyshev response and a ripple constant $\varepsilon = 0.1005$. The required Z_i, Z_{ij}, and R have been given in the second row of Table 1 in Section II.

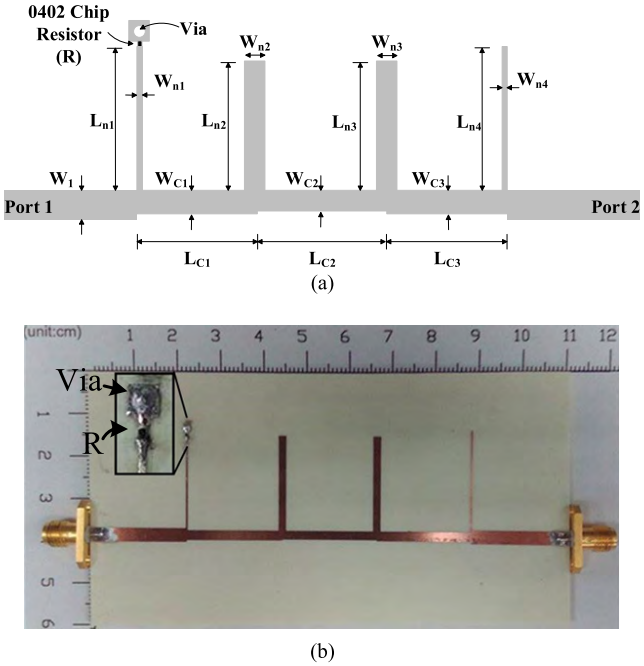

FIGURE 17. (a) Layout and (b) photograph of the microstrip ABSF design example in Fig. 5 with $f_0 = 2$ GHz, FBW = 0.5 and $n = 4$. (Geometrical parameters: $W_1 = 3.3$, $W_{C1} = 2.4$, $W_{C2} = 2.2$, $W_{C3} = 2.4$, $W_{n1} = 0.4$, $W_{n2} = 1.8$, $W_{n3} = 1.8$, $W_{n4} = 0.4$, $L_{C1} = 21.8$, $L_{C2} = 21.8$, $L_{C3} = 21.8$, $L_{n1} = 21$, $L_{n2} = 22.3$, $L_{n3} = 22.3$, and $L_{n4} = 23.3$. Units in mm. 0402 chip component value: R = 510 Ω.)

By using a computer-aided design tool, e.g. ADS LineCalc, the corresponding line width and line length of each microstrip line section can be easily obtained and they are given in the filter layout in Fig. 17(a). The resistor R is implemented with a 510-Ω 0402 chip resistor because the required R = 516.85 Ω is not available in practice. Shown in Fig. 17(b) is the photograph of the fabricated microstrip ABSF, and the measured and EM simulated frequency responses are shown in Fig. 18. The EM simulation is done by the full-wave simulator Ansys HFSS. Good agreement between measured and EM simulated results is obtained. The measured $|S_{21}|$ exhibits a bandstop frequency response centered at 2 GHz as expected, and the measured stopband rejection is 60.7 dB at 2 GHz. The measured 30-dB rejection bandwidth is from 1.77 to 2.24 GHz or 23.5%, while the measured 40-dB rejection bandwidth is from 1.83 to 2.17 GHz or 17%. Good stopband selectivity is achieved and the shape factor, i.e., RBW_{3-dB}/RBW_{30-dB} is 2.1. Notably, wideband impedance matching is obtained at Port 1 and the measured $|S_{11}|$ is better than −11.2 dB from dc to the highest measurement frequency of 8 GHz. This is because the resistor R can also absorb the input power at the harmonic resonances. In addition, the measured $|S_{11}|$ within the 30-dB rejection bandwidth is better than −13 dB. Shown in Fig. 18(c) is the power dissipation of this wideband ABSF when the input is at Port 1. The measured power dissipation is better than 95% from 1.66 to 2.38 GHz, and the corresponding fractional bandwidth is 35.6%.

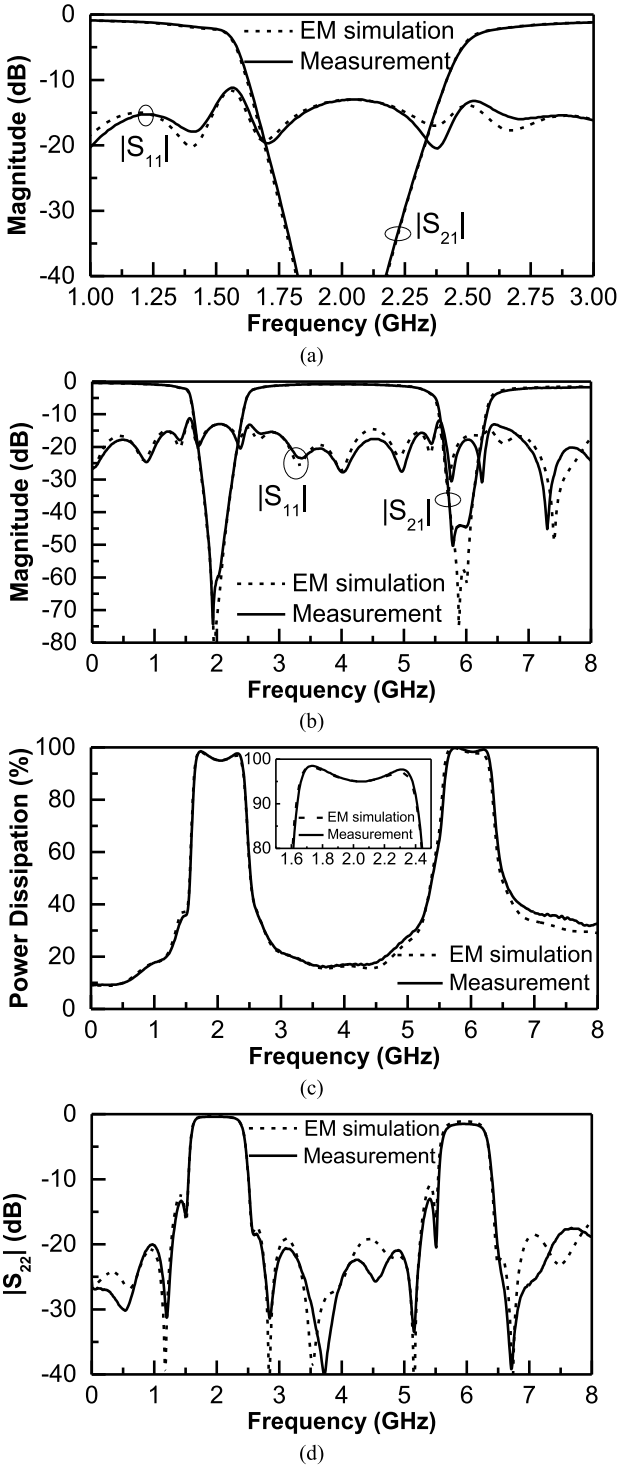

FIGURE 18. Measured and EM simulated results of the microstrip ABSF design example in Fig. 5 with $f_0 = 2$ GHz, FBW = 0.5 and $n = 4$. (a) Narrowband and (b) wideband S-parameter frequency responses, and (c) power dissipation frequency responses when the input is at Port 1. (d) $|S_{22}|$ frequency response.

In addition to the wide stopband and high level of stopband power dissipation, the proposed microstrip ABSF also exhibits low passband insertion loss with good passband impedance matching. The measured passband insertion loss

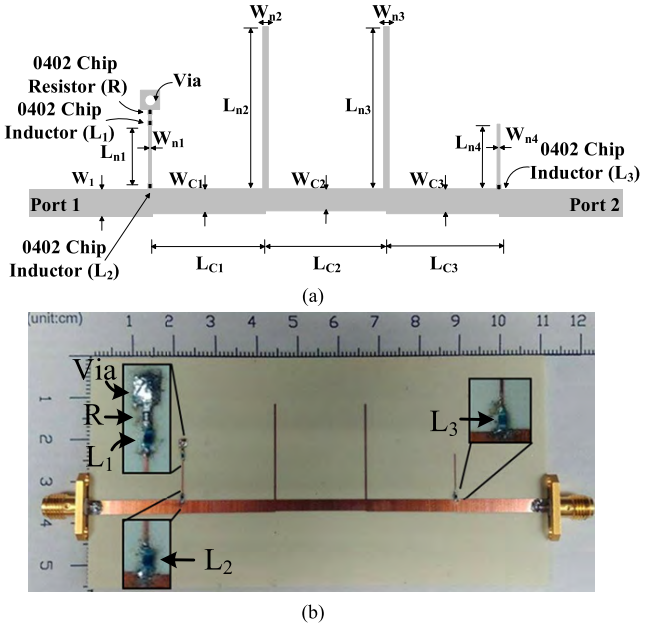

FIGURE 19. (a) Layout and (b) photograph of the modified design-I of proposed microstrip ABSF design example in Fig. 11 with $f_0 = 2$ GHz, FBW = 0.3, and $n = 4$. (Geometrical parameters: $W_1 = 3.3$, $W_{C1} = 3$, $W_{C2} = 2.8$, $W_{C3} = 3$, $W_{n1} = 0.26$, $W_{n2} = 0.4$, $W_{n3} = 0.4$, $W_{n4} = 0.26$, $L_{C1} = 21.9$, $L_{C2} = 21.9$, $L_{C3} = 21.9$, $L_{n1} = 8.4$, $L_{n2} = 23.1$, $L_{n3} = 23.1$, and $L_{n4} = 9.4$. Units in mm. 0402 chip component values: R = 1.5 kΩ, $L_1 = 8.7$ nH, $L_2 = 8.7$ nH, and $L_3 = 12$ nH.)

is within 1 dB from dc to 1.1 GHz and from 3.2 to 4.59 GHz, while the measured passband return loss is better than 16.9 dB in the same frequency range. On the other hand, the measured passband insertion loss is within 1.5 dB from dc to 1.32 GHz and from 2.82 to 5.05 GHz, while the measured passband return loss is greater than 15.3 dB in the same frequency range.

The measured and EM simulated output reflection coefficients of this microstrip ABSF are shown in Fig. 18(d). The input power at Port 2 is mostly reflected within the stopband as expected because the resistor R is only introduced to the first stub near Port 1.

B. CASE 2: FBW = 0.3 and n = 4

Next, the modified design-I of proposed ABSF with moderate bandwidth in Fig. 11 of Section II.C is implemented. The filter specifications are: $f_0 = 2$ GHz, FBW = 0.3, $n = 4$, and $Z_0 = 50\ \Omega$. Again, the filter is designed based on the optimal microwave BSF with a Chebyshev response and a ripple constant $\varepsilon = 0.1005$, but the first and last open stubs are replaced by the inductively loaded ones as shown in Fig. 10. By setting $Z_{iL} = 139.3\ \Omega$, all the other circuit parameters can be calculated accordingly as given in Section II.C. The ABSF is implemented using the same RO4350B substrate and the corresponding microstrip filter layout is shown in Fig. 19(a). The Murata LQW15AN series 0402 wirewound chip inductor is used to implement the inductive loadings because a high self-resonant frequency is required to extend the upper passband. The value of lumped chip inductors are

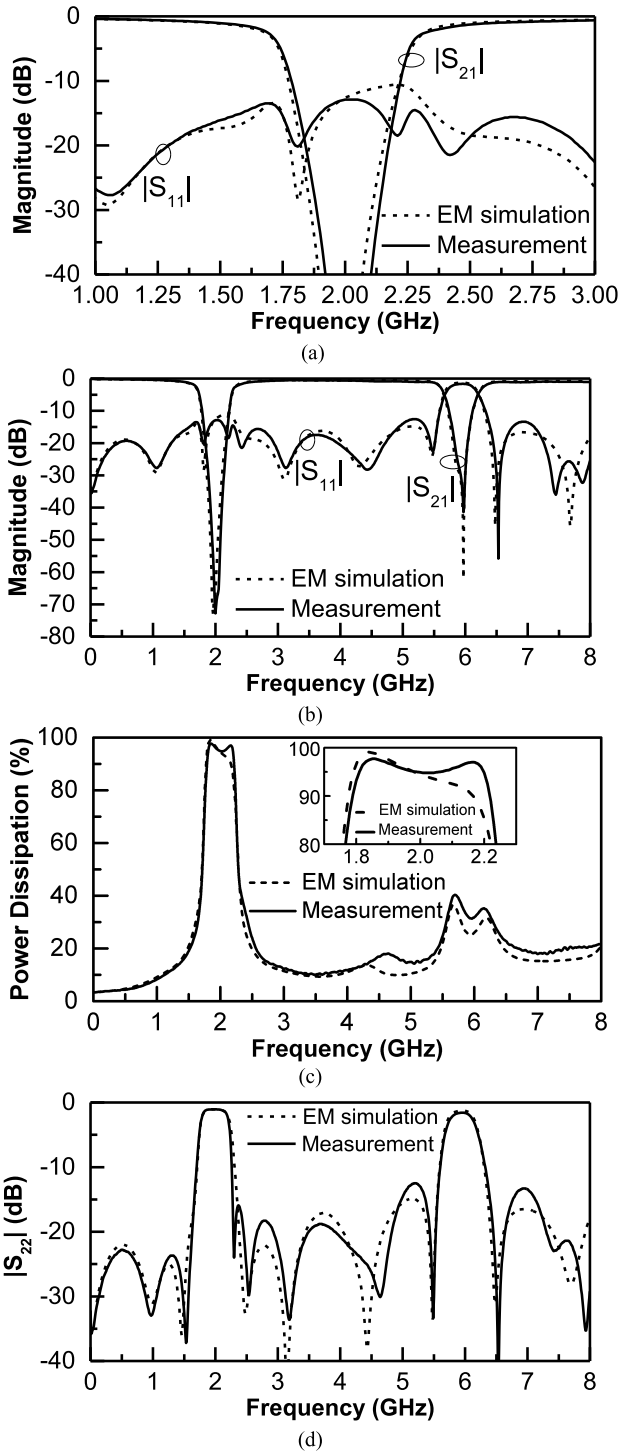

FIGURE 20. Measured and EM simulated results of the modified design-I of proposed microstrip ABSF in Fig. 11 with $f_0 = 2$ GHz, FBW = 0.3 and $n = 4$. (a) Narrowband and (b) wideband S-parameter frequency responses, and (c) power dissipation frequency responses when the input is at Port 1. (d) $|S_{22}|$ frequency response.

properly selected to take the parasitic effects into account, and they are given in the caption of Fig. 19. In addition, a 0402 resistor of 1.5 kΩ is used for R because the designed value of 1499 Ω is not available.

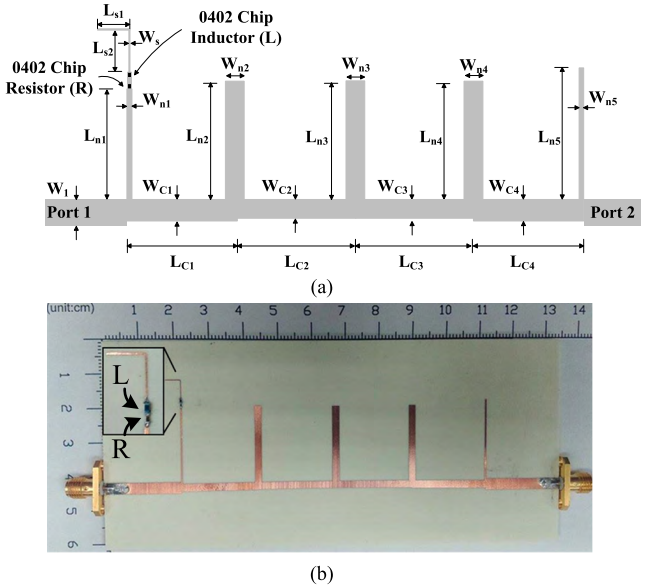

FIGURE 21. (a) Layout and (b) photograph of the modified design-III of proposed microstrip ABSF design example in Fig. 16 with $f_0 = 2$ GHz, FBW = 0.5 and $n = 5$. (Geometrical parameters: $W_1 = 3.3$, $W_{C1} = 2.3$, $W_{C2} = 2.1$, $W_{C3} = 2.1$, $W_{C4} = 2.3$, $W_{n1} = 0.45$, $W_{n2} = 2$, $W_{n3} = 2.2$, $W_{n4} = 2$, $W_{n5} = 0.45$, $W_s = 0.2$, $L_{C1} = 21.6$, $L_{C2} = 22.8$, $L_{C3} = 22.8$, $L_{C4} = 21.6$, $L_{n1} = 21.5$, $L_{n2} = 22.3$, $L_{n3} = 22.2$, $L_{n4} = 22.3$, $L_{n5} = 23.4$, $L_{s1} = 4.4$, and $L_{s2} = 5$. Units in mm. 0402 chip component values: R = 500 Ω and $L = 15$ nH.)

Shown in Fig. 20 are the measured and EM simulated frequency responses. The measured $|S_{21}|$ exhibits a bandstop frequency response with an absorptive stopband, and the measured rejection is 72.77 dB at $f = 2$ GHz. The measured 30-dB rejection bandwidth is from 1.89 to 2.13 GHz or 11.9 %, while the measured 40-dB rejection bandwidth is from 1.93 to 2.10 GHz or 8.4 %. Good frequency selectivity is achieved and the roll-off rate in the transition band from 10 to 30 dB rejection is better than 2 dB per 10 MHz. The measured $|S_{11}|$ is better than −12.9 dB from dc to 5.56 GHz. On the other hand, the measured passband insertion loss is within 1 dB from dc to 1.48 GHz and from 2.61 to 5.16 GHz. Shown in Fig. 20(c) is the power dissipation of this ABSF with the input at Port 1. The measured power dissipation is better than 90% from 1.79 to 2.22 GHz.

C. CASE 3: FBW = 0.5 and n = 5

The frequency selectivity of proposed wideband ABSF can be improved by using more stubs at the expense of a larger circuit area and a higher passband insertion loss. Although the maximal reflection coefficient increases as n increases, the modified design-III proposed in Section II.D can help reduce $|S_{11}|$ and improve $|S_{21}|$. The design example with $f_0 = 2$ GHz, $FBW = 0.5$ and $n = 5$ in Fig. 16 is also implemented in microstrip form using the same substrate. The circuit model is shown in Fig. 15, and the corresponding circuit layout is shown in Fig. 21(a) with the circuit photograph in Fig. 21(b). The Murata LQW15AN series 0402 wirewound chip inductor of 15 nH is used to realize L, and a 0402 resistor of 500 Ω is chosen for the resistor R. The λ/4 microstrip open stub behind the resistor R is bent to save some circuit area.

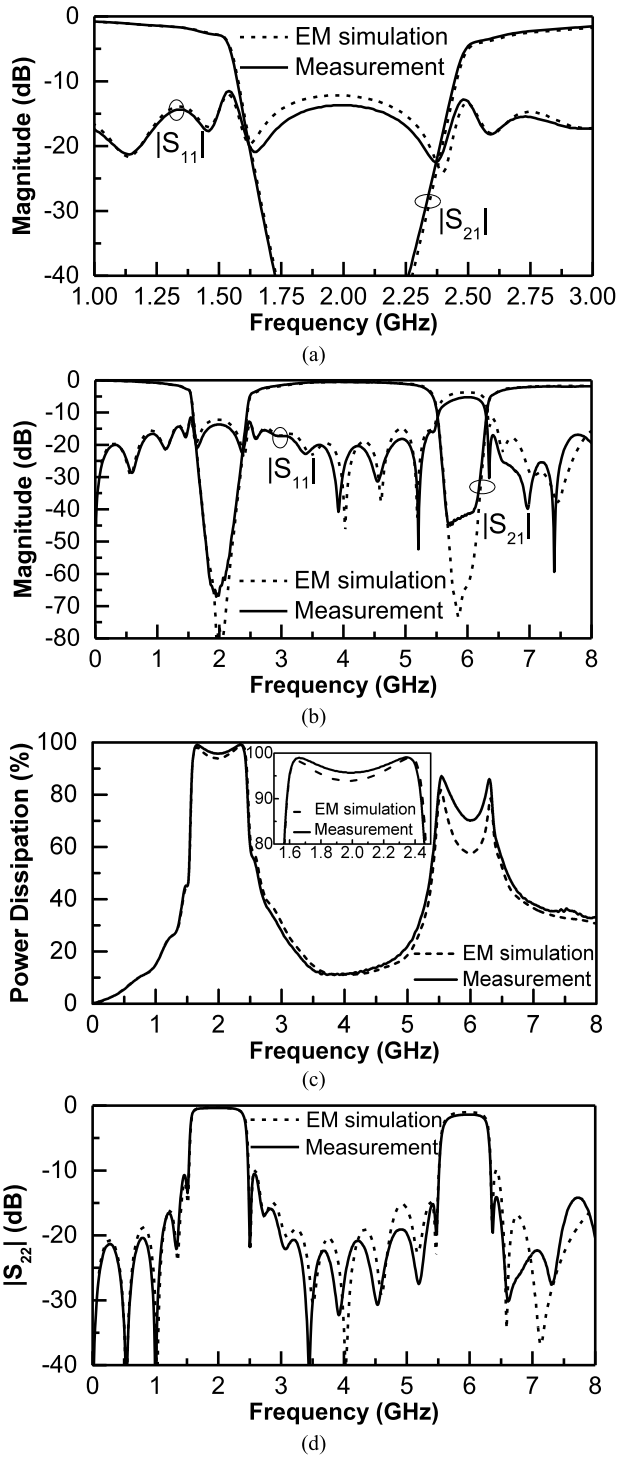

FIGURE 22. Measured and EM simulated results of the modified design-III of proposed microstrip ABSF in Fig. 16 with $f_0 = 2$ GHz, $FBW = 0.5$ and $n = 5$. (a) Narrowband and (b) wideband S-parameter frequency responses, and (c) power dissipation frequency responses when the input is at Port 1. (d) $|S_{22}|$ frequency response.

According to the measured and EM simulated results in Fig. 22, the measured $|S_{21}|$ features a rejection of 65.7 dB

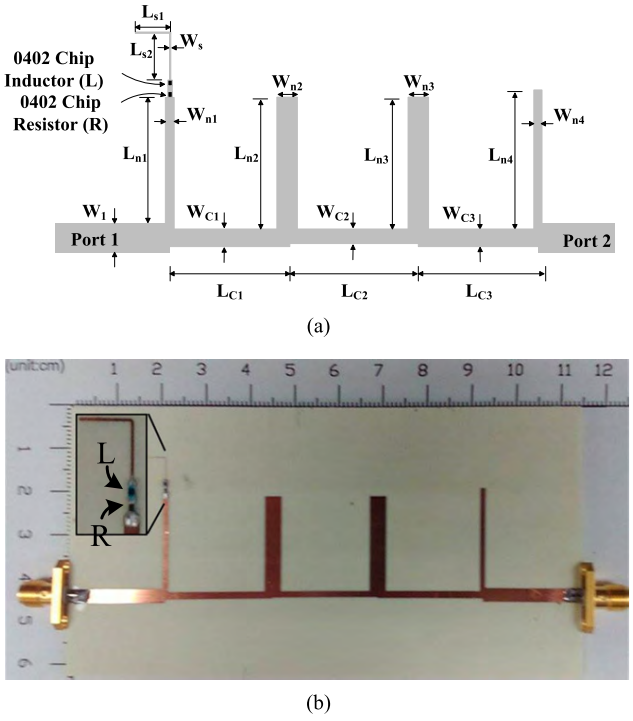

FIGURE 23. (a) Layout and (b) photograph of the modified design-III of proposed microstrip ABSF with $f_0 = 2$ GHz, FBW = 0.7 and $n = 4$. (Geometrical parameters: $W_1 = 3.3$, $W_{C1} = 1.8$, $W_{C2} = 1.6$, $W_{C3} = 1.8$, $W_{n1} = 1.25$, $W_{n2} = 3.8$, $W_{n3} = 3.8$, $W_{n4} = 1.25$, $W_s = 0.2$, $L_{C1} = 23.6$, $L_{C2} = 23.7$, $L_{C3} = 23.6$, $L_{n1} = 22$, $L_{n2} = 21.8$, $L_{n3} = 21.8$, $L_{n4} = 22.8$, $L_{s1} = 4.4$, and $L_{s2} = 5$. Units in mm. 0402 chip component values: R = 240 Ω and L = 15 nH.)

at $f_0 = 2$ GHz. The measured 30-dB rejection bandwidth is from 1.68 to 2.32 GHz or 32.4 %, while the measured 40-dB rejection bandwidth is from 1.73 to 2.26 GHz or 26.5 %. The shape factor (RBW_{3-dB}/RBW_{30-dB}) is 1.7, which is obviously smaller than that of the design example in Fig. 18 of Section III.A with the same FBW but fewer number of stubs. The roll-off rate in the transition band from 10 to 30 dB rejection is better than 1.67 dB per 10 MHz. An absorptive stopband is again achieved and the measured $|S_{11}|$ is better than −11.5 dB from dc to 5.52 GHz. The measured power dissipation is better than 90% from 1.59 to 2.43 GHz according to Fig. 22(c). As for the passband, the measured insertion loss is within 1 dB from dc to 1.09 GHz and from 3.25 to 4.89 GHz.

D. CASE 4: FBW = 0.7 and n = 4

Although the maximal input reflection coefficient and minimum passband insertion loss of proposed ABSF increases as FBW increases according to Fig. 7 in Section II.B, the modified design-III in Section II.D can be used to reduce the maximal $|S_{11}|$ and passband insertion loss for proposed wideband ABSF designs. Here, a design example with $f_0 = 2$ GHz, FBW = 0.7 and $n = 4$ is implemented in microstrip form using the same substrate. The required line impedances are those in the third row of Table 1 in Section II.B. A series inductor L of 15 nH along with an open stub of line

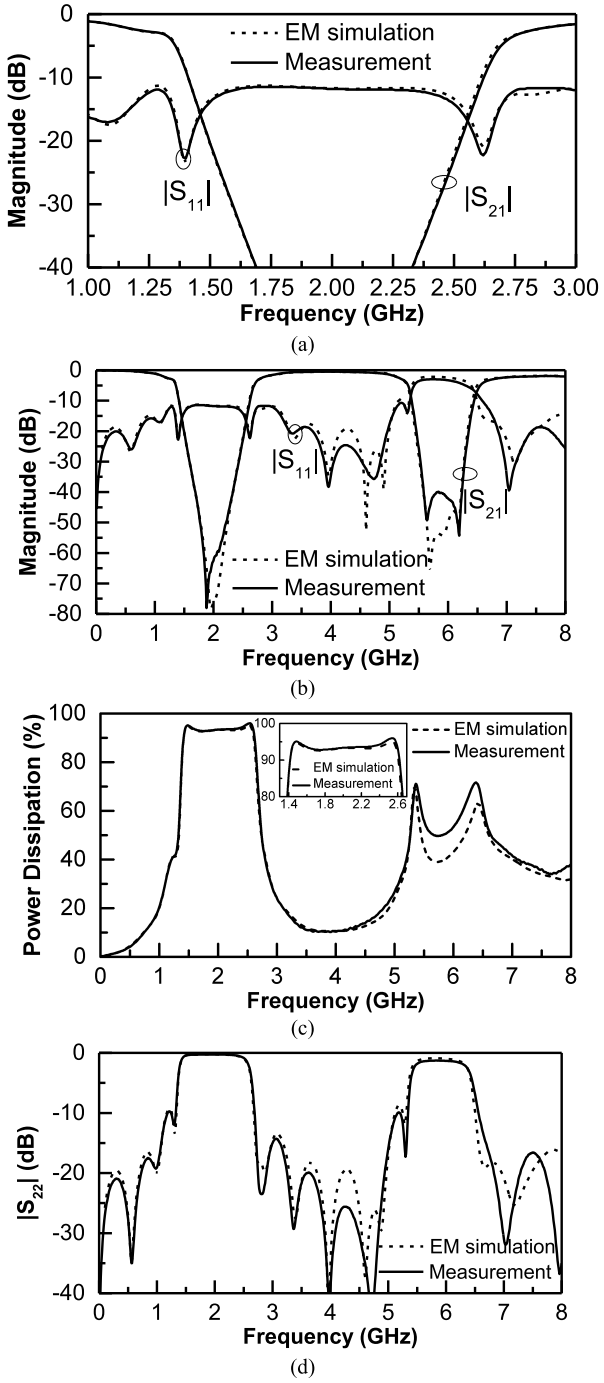

FIGURE 24. Measured and EM simulated results of the modified design-III of proposed microstrip ABSF with $f_0 = 2$ GHz, FBW = 0.7 and $n = 4$. (a) Narrowband and (b) wideband S-parameter frequency responses, and (c) power dissipation frequency responses when the input is at Port 1. (d) $|S_{22}|$ frequency response.

impedance $Z_{SL} = 147.9\ \Omega$ and electrical length $\theta_{SL} = 38.1°$ at $f_0 = 2$ GHz is introduced after the 240-Ω resistor R. The corresponding circuit layout and circuit photograph are shown in Fig. 23(a) and Fig. 23(b), respectively.

Shown in Fig. 24 are the measured and EM simulated results. The measured stopband rejection is 62.5 dB at $f_0 = 2$ GHz, and the measured maximal stopband

TABLE 4. Performance comparison with other related recent works.

Parameters	[11]	[16]	[23]	[22]	This Work (Fig.20)	This Work (Fig. 24)
Process	PCB	LTCC	LTCC	PCB	PCB	PCB
Topology	Coupled-Line ABSF	1st-order Lumped ABSF	2nd-order Lumped ABSF	Series-Cascaded ABSF	Stub ABSF	Stub ABSF
f_0	2 GHz	1 GHz	1 GHz	1.95 GHz	2 GHz	2 GHz
10-dB Rejection Bandwidth	2%	36.4%	*26.8%	N.A.	21.4%	63%
20-dB Rejection Bandwidth	0.9%	*10%	12%	*4.6%	15.9%	52.4%
30-dB Rejection Bandwidth	0.2%	3.4%	*4%	*3%	11.9%	42%
40-dB Rejection Bandwidth	N.A.	*1.6%	1.6%	N.A.	8.4%	31.8%
Max. Rejection	34.83 dB	>60 dB	>60 dB	>55 dB†	72.8 dB	78.1 dB
Roll-Off Rate from 10 to 30-dB Rejection	>0.95 dB/MHz	*>0.12 dB/MHz	*>0.15 dB/MHz	*>0.40 dB/MHz	>0.20 dB/MHz	>0.11 dB/MHz
Min. Return Loss	>17.5 dB from dc to 5.56 GHz	*>13 dB from dc to 1.75 GHz	*>10.5 dB from dc to 1.68 GHz	N.A.	>12.9 dB from dc to 5.56 GHz	>11.5 dB from dc to 5.14 GHz

*Estimated from graph
†Equal-ripple stopband

rejection is 78.1 dB at 1.88 GHz. The measured 30-dB rejection bandwidth is from 1.6 to 2.43 GHz or 42 %, while the measured 40-dB rejection bandwidth is from 1.69 to 2.33 GHz or 31.8%. To the best of our knowledge, this is the widest stopband bandwidth ever reported for ABSF designs. The measured $|S_{11}|$ is better than -11.5 dB from dc to 5.14 GHz, which leads to effective power absorption and the measured power dissipation when the input is at Port 1 is better than 90% from 1.42 to 2.61 GHz. Regarding the passband, the measured passband insertion loss is within 1 dB from dc to 0.96 GHz and from 3.18 to 4.82 GHz.

Shown in Table 4 is the performance comparison of proposed wideband ABSFs with other related recent works. The proposed design based on stub BSF can achieve much larger rejection bandwidth than other previous works on wideband ABSF designs including the bandwidth-enhanced lumped-element ABSF design in [23] and the series-cascaded ABSF design in [22]. Even with a much larger stopband bandwidth, the proposed wideband ABSFs still demonstrate good frequency selectivity, which can be observed from the comparison of the minimum roll-off rate from 10 to 30 dB rejection. Although the frequency selectivity of the series-cascaded ABSF design is much better than the proposed ones, it is achieved at the expense of an equal-ripple stopband.

Although the proposed wideband ABSF design requires tuning of the resistor R to achieve good overall input impedance matching, this is the only element to be tuned while all other circuit parameters can be obtained using closed-form design formulae. This makes the design of proposed wideband ABSF very efficient. Also, tuning of the resistor R gives designers the freedom to trade off between the return loss at f_0 and the minimum in-band return loss depending on the application requirement.

According to Table 4, the proposed ABSF can achieve much larger realizable stopband bandwidth than our previous work [11] using a similar design concept, but the input reflection coefficient achieved is not as good as [11]. This is due to the fundamental limit given by the Bode-Fano criterion [29], [30]. Anyway, even though the ideal circuit of some previous works on ABSF designs (e.g., [2]–[6], [16]) can achieve perfect input matching (i.e., $S_{11} = 0$ at all frequencies), due to parasitic effects they do not achieve perfect input matching in practice and the measured return loss is usually between 10 to 20 dB around f_0. According to the analysis in Fig. 7 and 8, the reflection coefficient of proposed ABSF is related to the stopband bandwidth and filter order. Better return loss can be achieved by choosing a smaller stopband bandwidth and a lower filter order.

IV. CONCLUSION

In this work, a simple and effective way to design wideband bandstop filters with an absorptive stopband is proposed. Analytical design equations are established to allow the direct synthesis of proposed wideband ABSF according to the desired specifications. Good stopband rejection, low input reflection coefficient, and high level of input power dissipation within the stopband are achieved. In addition, wide passbands with low passband insertion loss and good impedance matching are also obtained. The proposed wideband ABSF can achieve 30-dB stopband bandwidths ranging from about 12% to 42%, which is much larger than conventional designs. Better selectivity can also be easily achieved by extending the filter order. It can be used in applications where a proper passband and a wideband absorption of signal/interference are required.

ACKNOWLEDGMENT

S.-H. Chien was with the Department of Electrical Engineering, National Central University, Taoyuan 32001, Taiwan.

REFERENCES

[1] D. R. Jachowski, "Passive enhancement of resonator Q in microwave notch filters," in *IEEE MTT-S Int. Microw. Symp. Dig.*, Jun. 2004, pp. 1315–1318.
[2] D. R. Jachowski, "Compact, frequency-agile, absorptive bandstop filters," in *IEEE MTT-S Int. Microw. Symp. Dig.*, Jun. 2005, pp. 513–516.
[3] H. W. Bode, "Wave filter," U.S. Patent 2 035 258, Mar. 24, 1936.
[4] H. W. Bode, "Wave filter," U.S. Patent 2 002 216, May 21, 1935.
[5] A. C. Guyette, I. C. Hunter, R. D. Pollard, and D. R. Jachowski, "Perfectly-matched bandstop filters using lossy resonators," in *IEEE MTT-S Int. Microw. Symp. Dig.*, Jun. 2005, pp. 517–520.
[6] M. A. Morgan and T. A. Boyd, "Theoretical and experimental study of a new class of reflectionless filter," *IEEE Trans. Microw. Theory Techn.*, vol. 59, no. 5, pp. 1214–1221, May 2011.

[7] M. A. Morgan and T. A. Boyd, "Reflectionless filter structures," *IEEE Trans. Microw. Theory Techn.*, vol. 63, no. 4, pp. 1263–1271, Apr. 2015.
[8] J. Lee, T. C. Lee, and W. J. Chappell, "Lumped-element realization of absorptive bandstop filter with anomalously high spectral isolation," *IEEE Trans. Microw. Theory Techn.*, vol. 60, no. 8, pp. 2424–2430, Aug. 2012.
[9] Y. Morimoto, T. Yuasa, T. Owada, and M. Miyazaki, "Multi-harmonic absorption filter using quasi-multilayered striplines," in *IEEE MTT-S Int. Microw. Symp. Dig.*, Jun. 2014, pp. 1–3.
[10] J.-Y. Shao and Y.-S. Lin, "Millimeter-wave bandstop filter with absorptive stopband," in *IEEE MTT-S Int. Microw. Symp. Dig.*, Jun. 2014, pp. 1–4.
[11] J.-Y. Shao and Y.-S. Lin, "Narrowband coupled-line bandstop filter with absorptive stopband," *IEEE Trans. Microw. Theory Techn.*, vol. 63, no. 10, pp. 3469–3478, Oct. 2015.
[12] J.-C. S. Chieh and J. Rowland, "Quasi-lumped element bridged-T absorptive bandstop filter," *IEEE Microw. Wireless Compon. Lett.*, vol. 26, no. 4, pp. 264–266, Apr. 2016.
[13] T. Snow, J. Lee, and W. J. Chappell, "Tunable high quality-factor absorptive bandstop filter design," in *IEEE MTT-S Int. Microw. Symp. Dig.*, Jun. 2012, pp. 1–3.
[14] B. Kim, J. Lee, J. Lee, B. Jung, and W. J. Chappell, "RF CMOS integrated on-chip tunable absorptive bandstop filter using Q-tunable resonators," *IEEE Trans. Electron Devices*, vol. 60, no. 5, pp. 1730–1737, May 2013.
[15] T.-C. Lee, J. Lee, E. J. Naglich, and D. Peroulis, "Octave tunable lumped-element notch filter with resonator-Q-independent zero reflection coefficient," in *IEEE MTT-S Int. Microw. Symp. Dig.*, Jun. 2014, pp. 1–4.
[16] T.-H. Lee, B. Kim, K. Lee, W. J. Chappell, and J. Lee, "Frequency-tunable low-Q lumped-element resonator bandstop filter with high attenuation," *IEEE Trans. Microw. Theory Techn.*, vol. 64, no. 11, pp. 3549–3556, Nov. 2016.
[17] J.-C. S. Chieh and J. Rowland, "A fully tunable C-band reflectionless bandstop filter using L-resonators," in *Proc. 46th Eur. Microw. Conf.*, Oct. 2016, pp. 131–133.
[18] D. Psychogiou, R. Gomex-Garcia, and D. Peroulis, "Acoustic wave resonator-based absorptive bandstop filters with ultra-narrow bandwidth," *IEEE Microw. Wireless Compon. Lett.*, vol. 25, no. 9, pp. 570–572, Sep. 2015.
[19] D. Psychogiou, R. Gomez-García, and D. Peroulis, "Acoustic-wave-lumped-element-resonator filters with equi-ripple absorptive stopbands," *IEEE Microw. Wireless Compon. Lett.*, vol. 26, no. 3, pp. 177–179, Mar. 2016.
[20] I. Hunter, A. Guyette, and R. D. Pollard, "Passive microwave receive filter networks using low-Q resonators," *IEEE Microw. Mag.*, vol. 6, no. 3, pp. 46–53, Sep. 2005.
[21] D. R. Jachowski, "Cascadable lossy passive biquad bandstop filter," in *IEEE MTT-S Int. Microw. Symp. Dig.*, Jun. 2006, pp. 1213–1216.
[22] D. Psychogiou, R. Mao, and D. Perlious, "Series-cascaded absorptive notch-filters for 4G-LTE radios," in *IEEE Radio Wireless Symp. Dig.*, Jan. 2015, pp. 177–179.
[23] J. Lee, B. Kim, K. Lee, and W. J. Chappell, "Bandwidth-enhanced lumped-element absorptive bandstop filter topology and its application to LTCC bandstop filter design," *EuMA Int. J. Microw. Wireless Tech.*, vol. 7, no. 6, pp. 691–698, Dec. 2015.
[24] M. C. Horton and R. J. Menzel, "General theory and design of optimum quarter wave TEM filters," *IEEE Trans. Microw. Theory Techn.*, vol. MTT-13, no. 3, pp. 316–327, May 1965.
[25] M. C. Horton and R. J. Menzel, "The effectiveness of component elements in commensurate line length filters," *IEEE Trans. Microw. Theory Techn.*, vol. MTT-16, no. 8, pp. 555–557, Aug. 1968.
[26] O. P. Gupta and R. J. Menzel, "Design tables for a class of optimum microwave bandstop filters," *IEEE Trans. Microw. Theory Techn.*, vol. MTT-18, no. 7, pp. 402–404, Jul. 1970.
[27] J.-S. Hong, *Microstrip Filters for RF/Microwave Applications*, 2nd ed. Hoboken, NJ, USA: Wiley, 2011, ch. 6.
[28] K. Hettak, G. A. Morin, and M. G. Stubbs, "The integration of thin-film technologies for reduced-size MMICs," *IEEE Trans. Microw. Theory Techn.*, vol. 53, no. 1, pp. 283–291, Jan. 2005.
[29] H. W. Bode, *Network Analysis and Feedback Amplifier Design*. New York, NY, USA: Van Nostrand, 1945.
[30] R. M. Fano, "Theoretical limitations on the broadband matching of arbitrary impedances," *J. Franklin Inst.*, vol. 249, pp. 57–83, Jan. 1950.

SHIH-HUAN CHIEN was born in Changhua, Taiwan, in 1992. He received the B.S. degree in electrical engineering from National Chiayi University, Chiayi, Taiwan, in 2014, and the M.S. degree in electrical engineering from National Central University, Taoyuan, Taiwan, in 2017. He is currently an RF Engineer with Microelectronics Technology Inc., Hsinchu, Taiwan.

YO-SHEN LIN (M'04–SM'08) was born in Taipei, Taiwan, in 1973. He received the B.S. and M.S. degrees in electrical engineering and the Ph.D. degree in communication engineering from National Taiwan University, Taipei, in 1996, 1998, and 2003, respectively.

From 1998 to 2001, he was an RF engineer with Acer Communication and Multimedia Inc., Taipei, designing global system for mobile communication (GSM) mobile phones. From 2001 to 2003, he was with Chi-Mei Communication System Inc., Taipei, where he was involved with the design of LTCC RF transceiver module for GSM mobile applications. In 2003, he joined the Graduate Institute of Communication Engineering, National Taiwan University, as a Post-Doctoral Research Fellow, and became an Assistant Professor in 2004. Since 2005, he has been with the Department of Electrical Engineering, National Central University, Taoyuan, Taiwan, where he is currently a Professor and the Associate Chair of the department. From 2010 to 2013, he was also the Director of the Top University Program Office under the Research and Development Office of National Central University. He was a Guest Researcher with the Ferdinand-Braun-Institut, Leibniz-Institut für Höchstfrequenztechnik, Berlin, Germany, in 2008, and he was a Visiting Scholar with the Department of Electrical and Computer Engineering, University of California at San Diego, USA, from 2014 to 2015. He has authored or co-authored over 120 international journal and conference papers, and five granted U.S. patents. His research interests include the designs of miniature microwave passive component and highly integrated RF transceiver module for wireless communication applications. Since 2017, he has been the Vice Chair of the Taipei Chapter of the IEEE MTT-S.

Dr. Lin was a recipient of the Best Paper Award of the 2001 Asia-Pacific Microwave Conference, Taipei, the URSI Young Scientist Award presented at the 2005 URSI General Assembly, New Delhi, India, the URSI EMT-S Young Scientist Award presented at the 2007 URSI International Electromagnetic Symposium, Ottawa, Canada, the 2008 Exploration Research Award of the Pan Wen-Yuan Foundation, Taiwan, the 2012 Outstanding Young Electrical Engineer Award of the Chinese Institute of Electrical Engineering, Taiwan, and the Best Symposium Paper Award of the 2015 Asia-Pacific International Symposium on Electromagnetic Compatibility, Taipei.